Volume 12
Number 14
21 July 2025
Pages 4917–5434

Materials Horizons

rsc.li/materials-horizons

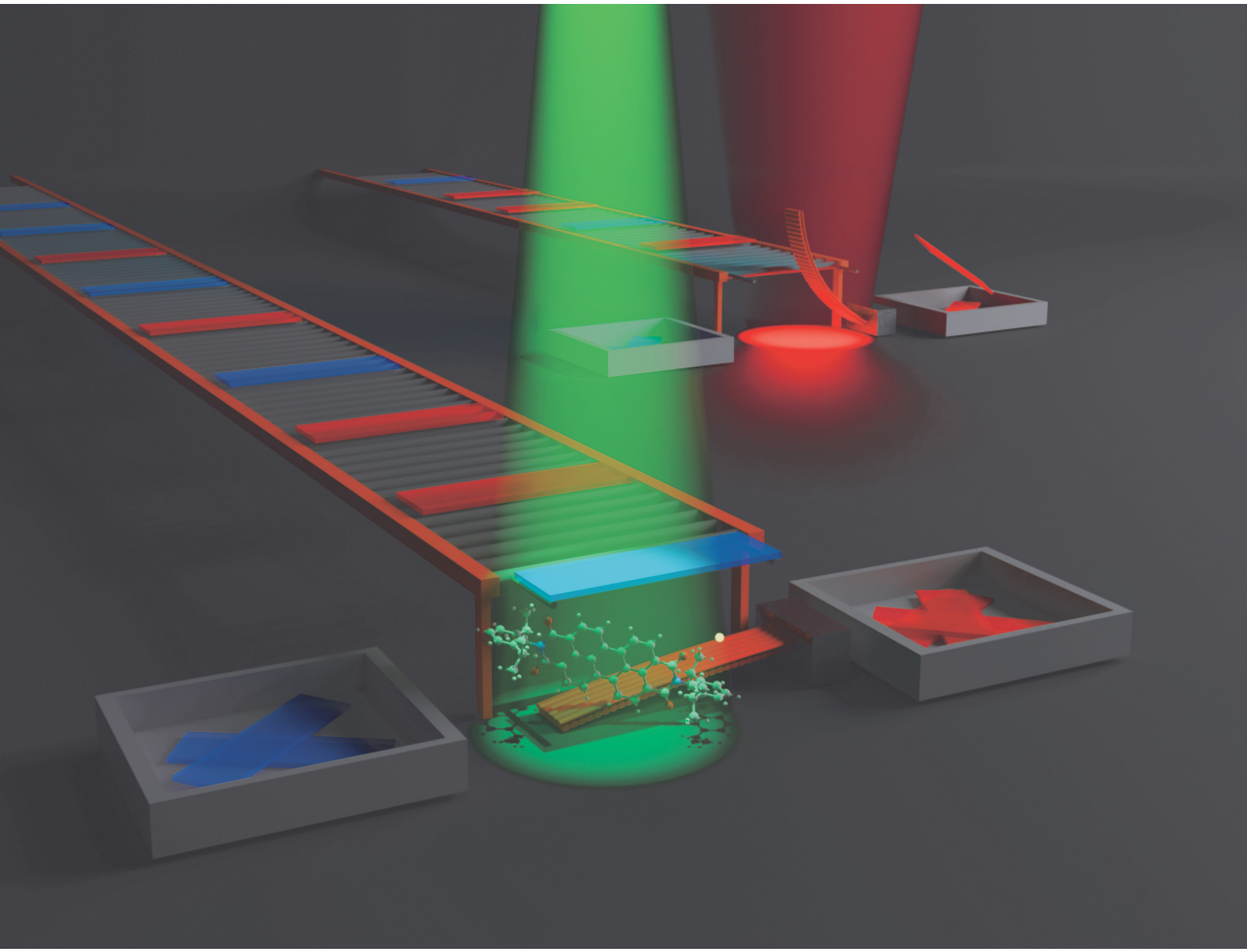

ISSN 2051-6347

ROYAL SOCIETY OF CHEMISTRY

COMMUNICATION
Carlos Sánchez-Somolinos *et al.*
Bridging sensing and action: autonomous object sorting by reprogrammable liquid crystal elastomers

Materials Horizons

ROYAL SOCIETY OF CHEMISTRY

COMMUNICATION

View Article Online
View Journal | View Issue

Cite this: *Mater. Horiz.*, 2025, **12**, 5149

Received 19th March 2025,
Accepted 22nd May 2025

DOI: 10.1039/d5mh00498e

rsc.li/materials-horizons

Bridging sensing and action: autonomous object sorting by reprogrammable liquid crystal elastomers†

Lorena Montesino, [a] María López-Valdeolivas,[a] Jesús I. Martínez [a] and Carlos Sánchez-Somolinos *[ab]

Achieving autonomy in soft robotics requires integrating sensing, planning, and actuation. Stimuli-responsive liquid crystal elastomers (LCEs) are promising for this purpose due to their intrinsic sensory capabilities, adaptability and integrability. Nevertheless, self-regulated LCE systems typically rely on single-mode bending actuators with feedback-type mechanisms, where deformation gradually increases with stimulus intensity but only causes a functional transition beyond a critical activation point. This enables autonomous switching between non-functional and functional states, however, their behavior remains reactive, limiting their ability to perform complex adaptive tasks. Here, we present a reprogrammable LCE actuator capable of autonomously sorting objects based on their green-light transmission properties. Using perylene diimide-doped LCEs and controlled green-light illumination, the actuator senses the optical properties of the object, establishing an actuation plan through spatial radical generation. Subsequent far-red irradiation triggers different actuation modes, enabling selective object sorting. This pattern-encoded actuation allows objects with different optical characteristics to trigger specific mechanical responses under identical illumination conditions. This single-material system, which is optically resettable, integrates sensory feedback, deliberative decision-making, and adaptive mechanical responses. Surpassing the reactive nature of conventional self-regulated LCE systems, our approach advances LCE-based robotics toward greater autonomy, aligning with the sense-plan-act paradigm.

New concepts

Herein, we introduce a reprogrammable liquid crystal elastomer (LCE) actuator capable of autonomously sorting objects based on their green-light transmission properties, marking a significant breakthrough from conventional self-regulated LCE systems. Unlike traditional LCE-based self-regulated devices that exhibit reactive responses, our approach integrates sensory input, deliberative decision-making, and multi-modal actuation within a single-material system. This advancement allows the actuator to not only respond to stimuli but also process optical information to determine actuation pathways. This is achieved through spatially controlled radical generation, wherein green-light illumination encodes different actuation plans by selectively creating radical species that absorb in the far-red region. Subsequent far-red irradiation triggers different mechanical responses depending on the optical properties of the object. This enables pre-programmed, differentiated deformation modes under identical stimulus conditions, facilitating sorting of objects based on their green-light transmission. This pattern-encoded actuation mechanism surpasses existing LCE-based feedback systems by introducing material-embedded decision-making, effectively bridging the gap between sensing and adaptive response. Additionally, the system is optically resettable, enabling repeated reconfiguration and therefore continuous sorting operation without external intervention. Our actuator represents a significant conceptual advance, aligning LCE-based soft robotics with the sense-plan-act paradigm, a fundamental principle in robotic autonomy.

Introduction

A robot can be defined as a human-conceived device designed to perform physically demanding or highly repetitive tasks.[1] To carry out these activities, traditional hard robots rely on hardware, typically consisting of a mechanical system including actuators, joints and links, sensors, control units, and a power source, as well as software that runs algorithms to determine how the robot executes its tasks.[1,2] Conceptually, this process can be subdivided into three steps: first, sensing an external stimulus coming from a physical system; second, planning an action based on the registered signal; and finally, actuation, which executes the task in the workspace, based on the established plan.[3] This sense-plan-act paradigm has allowed robots to excel in diverse applications, from assembly line automation to complex sorting systems, where robotic arms identify, categorize, and separate objects based on visual or sensory cues. This concept is schematically illustrated in Fig. 1(a).

[a] *Instituto de Nanociencia y Materiales de Aragón (INMA), CSIC-Universidad de Zaragoza, Departamento de Física de la Materia Condensada, Zaragoza, 50009, Spain. E-mail: carlos.s@csic.es*

[b] *Centro de Investigación Biomédica en Red de Bioingeniería, Biomateriales y Nanomedicina, Instituto de Salud Carlos III, Zaragoza, 50018, Spain*

† Electronic supplementary information (ESI) available. See DOI: https://doi.org/10.1039/d5mh00498e

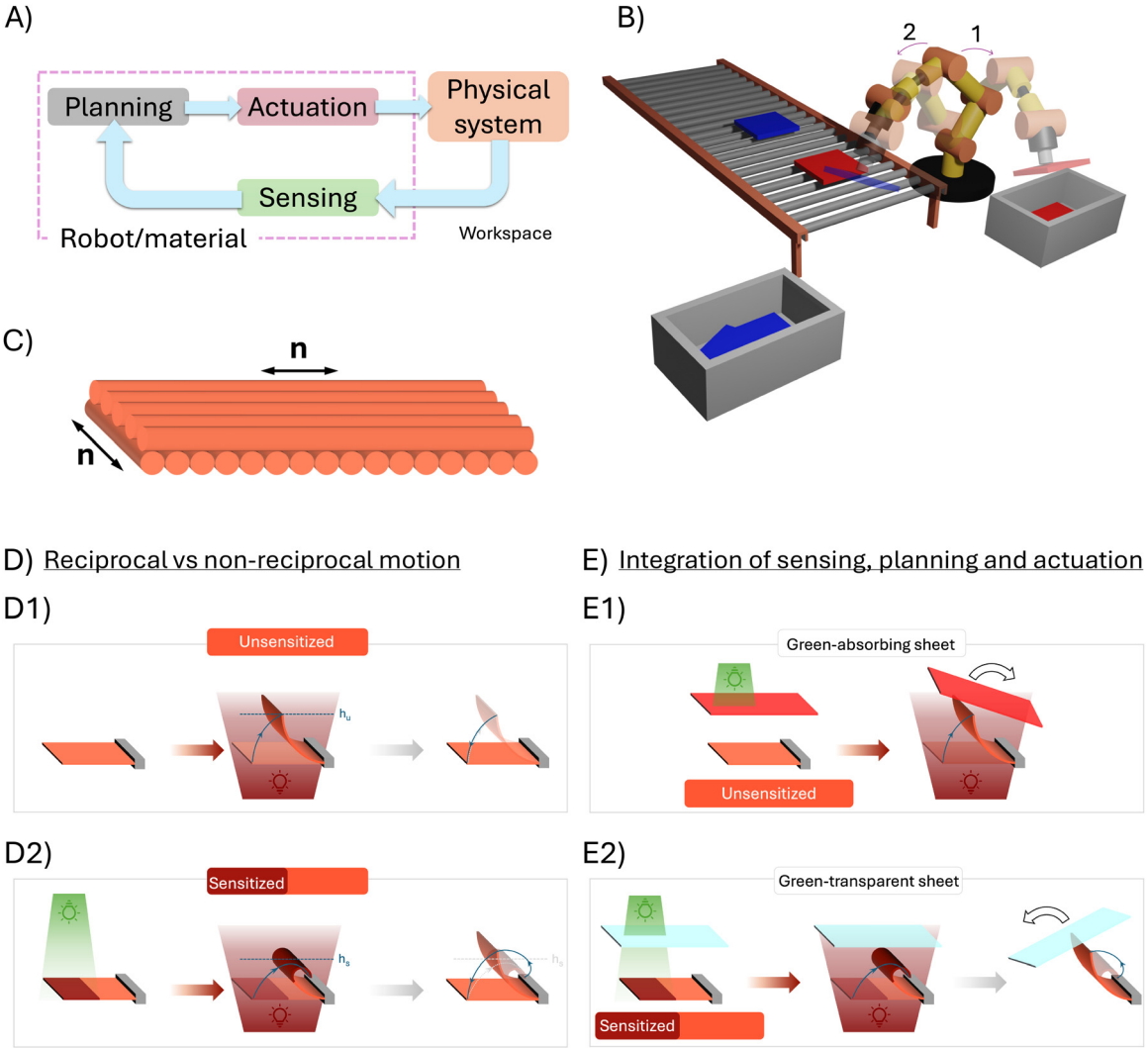

Fig. 1 Sorting LCE soft robot: concept, design and working principles. (a) Conceptual representation of the working principle of a robotic system. (b) Schematic diagram of a conventional industrial sorting line. It consists of a roller conveyor that transports items for sorting. Based on their color, the robotic arm can sort them to the right if they are red (1) or to the left if they are blue (2). (c) Conceptual representation of a 4D printed bimorph LCE actuator, with orthogonal alignment within the plane. (d) Operating principle of a 4D printed bimorph LCE actuator based on a perylene-based reconfigurable material. (i) When the LCE is in its unsensitized state, it describes a conventional bending motion under far-red light stimulation, with its tip reaching a maximum height, designated as h_u (the subscript 'u' refers to the unsensitized state). During unbending, when the far-red light is switched off, the tip closely follows the path taken during the bending process but in opposite direction, resulting in an overall reciprocal trajectory. (ii) On the other hand, when green light is used beforehand to sensitize the free-tip half of the actuator, the tip describes an overall non-reciprocal motion, bending when irradiated with far-red light and unbending when far-red light is switched off. In this case, the maximum height reached by the actuator, designated as h_s (the subscript 's' refers to the sensitized state), differs from the maximum height h_u attained by the unsensitized actuator under far-red light. (e) Integration of the sense-plan-act paradigm in the proposed sorting soft robot. The LCE actuator senses the green light transmission properties of the object placed on top and plans its response accordingly. When irradiated with far-red light, it sorts the object according to the plan established in the previous sensing step. (i) If the object blocks green light from reaching the LCE (*e.g.*, a red sheet), the actuator remains unsensitized and sorts the object moving it to the right during the bending phase of the actuator under far-red light. (ii) Conversely, if the object transmits green light (*e.g.*, a transparent sheet), the LCE becomes sensitized to far-red light in its free-tip half region and sorts the object moving it to the left during the unbending phase of the actuator, once the far-red light is switched off.

In contrast to the hard and non-flexible nature of conventional robotics, soft robotics emerged by integrating soft elements, such as silicone-based components, into traditional robot designs enabling greater customization, adaptability and safer interaction with their operating space.[4–6] Another promising direction within this field of soft robotics is the use of soft smart materials, which, with their ability to sense and accordingly respond to stimuli, offer basic forms of adaptation and self-regulation without circuitry.[7–9] Specifically, liquid crystal elastomers (LCEs) show great potential for these purposes. These systems are anisotropic elastomeric networks, bearing liquid crystalline units, known as mesogens, in their macromolecular structure. These stimuli-responsive materials undergo reversible order-to-disorder transitions when exposed to external

stimuli, leading to large, controlled and also reversible deformation, with significant potential for applications due to the wide variety of triggers to which they can respond, including thermal, light, magnetic and electrical.[10–19] Notably, this responsiveness allows them to interact with their surroundings, effectively sensing changes and adapting their response accordingly.[20–23]

As an important advancement in achieving robotic autonomy in LCE systems, Wani *et al.* developed a light-driven artificial flytrap, an autonomous soft device based on a light-sensitive LCE film mounted on the tip of an optical fiber. This artificial flytrap can close autonomously in the presence of an object. The working principle of this device is based on the photothermal bending of a splay-aligned LCE actuator under blue light, that is emitted through the optical fiber. When an object comes into the emission cone of the fiber, it reflects light on the LCE film, providing optical feedback that induces heating and thus a bending deformation that depends on the size of the object. Above a certain threshold value of the optical feedback that triggers the response in the film, the closing gesture leads to a gripper effect on the object. When the light is turned off, the LCE recovers its original shape, releasing the object it had captured. Therefore, the releasing step of the captured elements is driven by external intelligence.[24] In another recent example, Lyu *et al.* innovatively integrated sensing, signal processing and actuating functionalities by coupling a thermally sensitive LCE actuator patterned with a printed sensing electrode, this having a micro-gap at its center, which prevents current flow. When exposed to heat from a human finger, the LCE induces structure bending, and once a certain deformation threshold is exceeded, the electrode gap closes allowing current to flow. This current induces additional Joule heating, which further enhances the bending deformation. Notably, this effect persists even after the initial heat source, the finger, is removed. Eventually, the actuator bends to a stable angle as it reaches thermal equilibrium with the surrounding air.[25] This adaptive hybrid unit, which consists of an LCE actuator and a flexible electronic circuit, can use heat from the human touch to close the circuit and generate an electric signal, allowing the actuation of the system solely through an external electrical source. By combining multiple of these adaptive units, in this work, Lyu *et al.* successfully developed a biomimetic artificial Mimosa that responds to human touch. To return the system to its original relaxed state, the current must be actively switched off.

In the two previous examples, the actuators reactively bend when exposed to the external stimulus. This deformation gradually increases with stimulus intensity, but only when a specific activation threshold is exceeded, the system transitions into its functional state (gripping or retracting, respectively for each of the two previous examples). Below this threshold, partial bending occurs, but it remains insufficient to complete the intended function. This feedback-type response exemplifies self-regulated mechanisms where the systems continuously react to environmental cues but exhibit a transition between non-functional and functional states once a critical point is reached, demonstrating a reactive decision-making process that is embedded in the material response.

Despite these ongoing efforts to enhance the self-regulated and adaptive behavior of LCE systems through intelligent integration of sensing and actuation, their response patterns remain largely constrained to single-mode actuation. The employed systems primarily work through a consistent bending mode to execute the programmed function, gripping or retracting, and later, upon stimulus removal, recover their initial state by unbending following the same path in reverse. As a result, the overall deformation-relaxation behavior in these systems is inherently reciprocal, a characteristic typical of conventional LCEs.

The development of reconfigurable materials, such as reprogrammable LCEs, has introduced new opportunities for broadening the complexity of response patterns in LCE actuators. The ability to modify properties such as shape, stiffness, or optical characteristics in reprogrammable LCEs in a controlled manner, along with the capability to induce these modifications in different patterned configurations, provides access to multiple actuation modes within a single actuator, even when exposed to the same consistent stimulus. Additionally, reprogrammable LCEs can be dynamically adjusted and returned to their original state on demand.[26] This reversibility enables the reuse of the system, which can be reprogrammed with a different patterned modification, leading to a different actuation mode.[27–30] The ability to induce different modes of action within a single actuator, even under a constant stimulus, has been explored to recreate non-reciprocal movements, key components of locomotion in many organisms.[31] This principle has been actively pursued in soft robotics driving efforts to recreate biomimetic motions.[28] However, the use of these reconfigurable materials and their multi-mode capabilities in soft robotics has been limited to demonstrations of their principles of motion, with no reported practical proof-of-concept implementation of robotic functions.[31] Significant efforts need to be made for their integration into practical soft robotic systems.

Here, we present a reprogrammable LCE actuator capable of autonomously sorting objects based on their green-light transmission properties. Inspired by the operation of a sorting robot, which in its simplest form moves objects of two types to two different positions, this work leverages the intrinsic properties of reconfigurable materials to build an LCE-based system that autonomously sorts sheets based on their ability to transmit or block green light. To this end, we use a recently developed combination of LCE with a perylene diimide chromophore.[18] The exposure of this material to green light induces the generation of radical species (Sensing) that absorb in the far-red region, enabling reprogrammable multi-mode actuation. By restricting green illumination to a specific area of the actuator, a radical pattern forms. In contrast, completely blocking green light, prevents any radical formation. These two distinct material states, one with a radical pattern and one without, encode two different response plans (planning), dictating each a specific actuation mode upon subsequent photoactivation with far-red light. Upon irradiation with this wavelength, deformation occurs (actuation), according to the embedded radical species pattern. Through a careful system design and controlled illumination conditions, the LCE-based actuator can sense the

green-light transmission properties of the sheet to be sorted. This sensing encodes a plan that, upon subsequent far-red irradiation, triggers one of the two distinct actuation modes, selectively directing the sheets to two different locations based on their specific green-light transmission properties. This process effectively enables the system to function as an autonomous sorting device that integrates sensing, planning and actuation capabilities.

Results and discussion

Integration of sensing, planning and actuation. Design of a sorting soft robot

To demonstrate the integration of sensing, planning and actuation functions using a reprogrammable single-material soft actuator, we drew inspiration from the principle of operation of industrial sorting robots. In a typical industrial sorting line, a roller conveyor commonly transports objects to the working area where sorting occurs. An optical sensor scans the object, and its properties, such as color or shape, are analyzed. The signal gathered by the sensor is sent to a control unit, which uses specialized software to run the algorithm and plan the robot arm movement to the appropriate location, thus sorting the object based on its intrinsic properties. For simplicity, and to draw an analogy with the soft system developed in our work, described later, we focus on sorting robot arms with dual-mode actuation for two distinct types of objects, as schematically shown in Fig. 1(b). These robotic systems classify objects into two categories based on a property with two distinct values. For instance, a robot arm could detect the color of the object, directing one color to the left box and another color to the right.

To implement the soft robotic sorting system proposed in this work, we want to harness the advantages of a printable, reprogrammable LCE incorporating a perylene dye.[18] This material platform offers dual functionality: it enables programming the mechanical behavior through 4D printing and reconfiguration of the photoresponse to far-red light using green light. By leveraging these capabilities, we can manufacture actuators that can be later programmed to exhibit diverse and complex behaviors under far-red light of consistent intensity and irradiation time. For the sorting robot application pursued, we propose using a 4D printed bimorph LCE actuator, with orthogonal alignment directions in the plane, as schematically shown in Fig. 1(c). Upon exposure to a stimulus such as light-induced heat, which generates liquid crystal disorder, the bottom layer of this actuator, with its director aligned along the short axis, contracts along this direction and expands perpendicularly. In contrast, the top layer, with its director aligned along the long axis, contracts along the long axis and expands in the transverse direction. This anisotropic strain mismatch across the layered structure generates an upward bending moment, causing the actuator to deform out of plane to relieve the resulting internal stresses. Previous research has demonstrated that when appropriately programmed with green light in perylene diimide-based systems, this director configuration can produce non-reciprocal motions.[18] Preliminary experiments revealed significant differences in actuator bending induced by far-red light, depending on whether the sample had been previously sensitized to this wavelength with green light, as schematically shown in Fig. 1(d). During homogeneous photoinduced heating under far-red light irradiation, the unsensitized system bends with nearly uniform curvature. As a result, its tip, as shown in Fig. 1(d)-(i), increases its height during bending to a maximum height, designated as h_u ('u' referring to the unsensitized state), and moves toward higher positive x-values (to the right) until the temperature stabilizes. When light is switched off, and therefore the heating stimulus ceases, the system retraces its path along essentially the same trajectory, exhibiting an overall reciprocal motion. Notwithstanding, reconfigurability enables patterning of the material, making certain areas of the actuator more sensitive to the far-red light than others. Particularizing to the present case, the proposed bimorph actuator is half-patterned by irradiating only the free-tip half with green light as a preliminary step before far-red photoactuation. Consequently, the area sensitized with green light bends exhibiting a faster and more pronounced curvature when exposed to far-red light, as it contains the previously mentioned far-red light-absorbing radical species. In contrast, the half of the actuator closer to the anchor bends more slowly, following the typical dynamics of an unsensitized actuator. As a result, during this bending phase, the tip of the patterned actuator describes a markedly different trajectory compared to that of the unsensitized actuator. The maximum height reached during bending by the sensitized actuator, denoted as h_s ('s' referring to the sensitized state), is significantly shorter than h_u, as schematically shown in Fig. 1(d)-(ii). When the far-red light is switched off, the system cools down and initiates the unbending process. During this phase, the tip of the sensitized actuator initially moves to higher positive x-values (*i.e.*, moving to the right) until it reaches a maximum value. At this maximum position, the tip then begins a steady movement toward decreasing x-values (*i.e.*, moving to the left). Notably, as observed in our preliminary experiments (and later demonstrated in this work), its trajectory gradually converges toward that of the unsensitized actuator during unbending, reaching in this motion heights notably greater than h_s. Eventually, the actuator returns to its original state, as schematically illustrated in Fig. 1(d)-(ii).

By closely examining the trajectories of both unsensitized and sensitized actuators under the same far-red light stimulus, we observe that the tip of the unsensitized actuator enters the region defined by the height range between h_s and h_u while bending to the right, whereas the tip of the sensitized actuator enters this region only while unbending to the left. This dual-mode actuation feature enables the actuator to interact differently with an object placed in this region, controlling its displacement to the right or the left based on the sensitization of the actuator. Bearing this in mind, if an object that prevents green-light transmission, such as a red sheet, is placed between a green light source and the actuator, at a height slightly above

h_s, the green light will not reach the actuator, preventing radical generation on it. Without radicals, the unsensitized actuator will heat uniformly under far-red irradiation, bending with consistent curvature throughout. As it reaches its maximum height during the bending process, the unsensitized actuator will contact the red sheet, pushing it to the right, as schematically shown in Fig. 1(e)-(i).

Conversely, if an object that allows green-light transmission, such as a transparent sheet, is placed between the green light source and the actuator, at the same height, slightly above h_s, the green light will pass through. This allows the actuator to receive green light on the free-tip half, generating radical species and sensitizing this region to the far-red light. As a result, the sensitized half of the actuator exhibits increased far-red absorption, leading to additional photoinduced heating and a faster and more pronounced bending curvature than the half of the actuator close to the anchor, as described earlier. Throughout this bending phase, the actuator remains always below h_s and, therefore, avoids contact with the sheet. Once the stimulus ceases, the actuator starts unbending. Based on the preliminary studies mentioned, the unbending path is different from the one traced during bending. During this unbending step, the tip of the LCE actuator eventually moves to the left. As it unbends, the tip enters the height range where the sheet is placed, comes into contact with it, and pushes it to the left, as schematically shown in Fig. 1(e)-(ii). After sorting the transparent sheet, a sufficient dose of far-red light should be applied to deplete the radicals and prepare the system for reuse.

Ink preparation

To make proof of concept of the proposed sorting device, we have selected direct ink writing (DIW) as the technique for preparing our actuators, as this method offers great design flexibility in terms of director patterns, lateral dimensions, and thickness without restrictions, all with great reproducibility.[13,32] Our ink formulation includes an acrylate-ended main-chain LC macromer as the LCE to ensure the proper rheology during printing. Additionally, it contains Perylene Orange (PO) as a photochromic dye and a photo-initiator (IRG369) to trigger the crosslinking of the acrylate-ended macromers, resulting in the formation of the LCE. Details on the chemical structure of the molecules used in this work are provided in Fig. 2(a).

Seeking an adequate LCE material for our purposes, our initial objective was to develop a printable ink that, upon photopolymerization, results in an LCE capable of performing non-reciprocal motion under tailored sensitization and excitation conditions. This motion should exhibit sufficiently distinct bending and unbending trajectories. By achieving this and positioning an object at the appropriate height, the unsensitized and the sensitized actuators would make contact with it during photoinduced bending and unbending steps, respectively, as described in the previous section, effectively executing the motions required for the sorting function.

Based on our previous knowledge of perylene-based LCEs with similar chromophore concentrations, far-red light at an intensity of 675 mW cm^{-2} has been shown to increase the temperature of PO-containing samples by 20 °C. However, this heating is significantly amplified, causing a rapid temperature rise of approximately 90 °C when the samples are previously exposed to green light.[18] In this work, to achieve the motions described in Fig. 1(d), and taking these heating temperatures as a reference, our initial objective is to develop a material having two key characteristics. First, the unsensitized state should exhibit a sufficient response within the temperature range reached under far-red irradiation. Second, the sensitized state should demonstrate a significantly larger mechanical response than the unsensitized state at slightly higher temperatures which can be quickly reached under far-red irradiation. This design aims for the unsensitized actuator to achieve sufficient displacement during the bending step, while the sensitized actuator undergoes a larger and faster deformation at this stage of actuation. This last effect could result in a sufficiently distinct motion during rapid photoinduced heating, ultimately leading to an overall non-reciprocal motion of large amplitude. To achieve this, we adopted the strategy of lowering the liquid crystal to isotropic transition temperature ($T_{LC\text{-}I}$) of the LCE, bringing it slightly above room temperature (RT), the temperature at which our experiments were conducted. Differently from the previous work mentioned above, in which a three-ring LC diacrylate was exclusively used as reactive mesogen (RM82), in this work an LC diacrylate (C6BAPE) with two aromatic rings was incorporated into the main chain, along with an LC diacrylate (RM257) that contains three rings.[18] The use of C6BAPE reduces the intermolecular forces between the polymer chains by decreasing the strength of the π–π coupling, as previously demonstrated by several authors.[33,34] C6BAPE was combined with RM257, in a 1 : 1 ratio, based on previous results indicating that the exclusive use of C6BAPE did not provide optimal alignment for printing the LCE precursor inks.[35] To ensure sufficient strain in the resultant LCE, oligomers were synthesized *via* the Michael addition of the *n*-butylamine to these reactive mesogens in a 1 : 1.02 molar ratio, as detailed in the Experimental Section. Together with IRG369 as a photo-initiator and PO as a photoactive unit, this formulation yielded the desired ink to be printed. DSC analysis revealed a $T_{LC\text{-}I}$ at 32 °C for the ink, along with a T_g of −23 °C (see Fig. S1, ESI†).

Manufacturing of the actuator and its characterization

Printing and photopolymerization process. The actuators were manufactured using a home-built 3D printer described in detail in the Experimental Section. The printer consists of a thermalized reservoir kept at 60 °C where the syringe with the ink is placed. The ink is extruded through a needle by the action of pressurized air, being the material deposited on top of PVA-coated glass slides. Ink filaments are deposited with a 200 μm spacing, favoring fusion just after deposition to generate a continuous film.

It is well-known that during printing, the polymer chains, and therefore, the mesogens, align along the movement direction of the needle due to the shear forces and/or the elongational flow.[13] This alignment of the LCE director along the printing direction enables digital control of the morphology of the printed elements

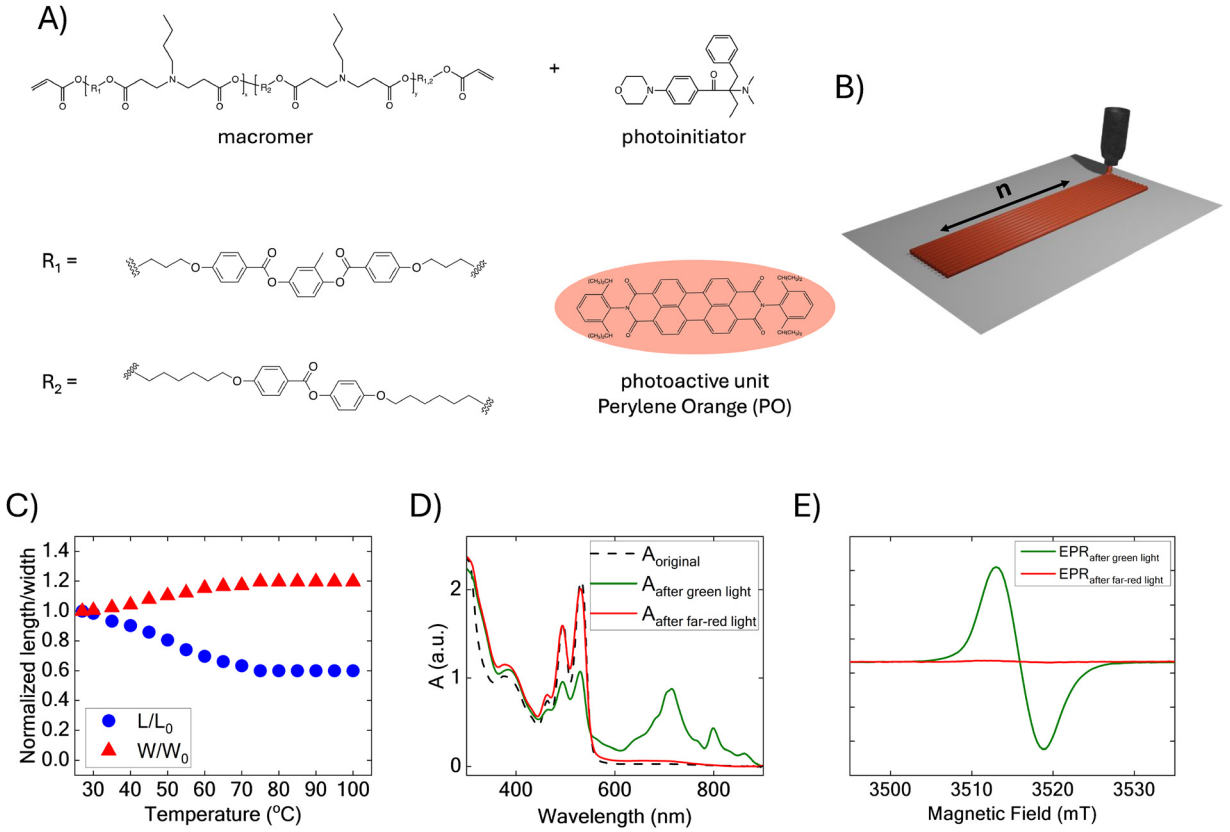

Fig. 2 Materials, manufacturing and characterization of the LCE. (a) Chemical structure of the ink components, including the reactive mesogens, the Perylene Orange chromophore and the photoinitiator IRG369. (b) Conceptual representation of the printing process of a single-layer uniaxial actuator. (c) Temperature dependence of the normalized length (blue dots) and width (red triangles) of a uniaxially oriented LCE strip (100 μm thick) with the director along its long axis and a 1 g weight attached to its free end, during the heating process. (d) Absorption spectra of a 100 μm thick actuator. The dashed black line corresponds to the initial spectrum, while the solid green line represents the spectrum after exposure to green light (525 nm) at an intensity of 100 mW cm^{-2} for 30 seconds. The solid red line depicts the spectrum following irradiation with far-red light (740 nm) at 450 mW cm^{-2} for 2 minutes, immediately after the green light exposure. (e) EPR spectra of the material under different irradiation conditions. The green EPR signal was the one registered after exposure to green light (525 nm, at an intensity of 100 mW cm^{-2} for 30 seconds), whereas the red one represents the signal detected after being irradiated with far-red light (740 nm) of 450 mW cm^{-2} for 2 minutes, immediately after the green light exposure.

through this printing technology. This was verified in our system using polarization optical microscopy (POM) (see Fig. S2, ESI†).

After printing, the elements were exposed to UV light to trigger the photopolymerization process, mediated by the photoinitiator IRG369. A color change was observed upon UV exposure, but the samples gradually returned to their original shade after a while, as previously described for a homologous perylene-containing system.[18] Once polymerized, gel fraction tests were performed on each batch, obtaining values close to 98%, demonstrating an efficient light-induced formation of the polymeric network.

Different shapes of actuators and director morphologies were printed to achieve the goals pursued in this work. First, single-layer uniaxial actuators (as schematically shown in Fig. 2(b)) were printed for the characterization and quantification of the optical and mechanical properties of the material. Besides, bimorph actuators with orthogonal director orientation within the plane were fabricated for application in the targeted sorting robot.

Thermal actuation. As discussed earlier, to achieve a large non-reciprocal motion, we targeted the preparation of a low-temperature actuation material that enables a rapid transition from the LC phase to the isotropic phase during the photoinduced heating step. To assess this thermomechanical performance, the temperature-dependent deformation of a uniaxial actuator was studied. This assessment aimed not only to verify contraction at temperatures near RT but also to ensure that the presence of the chromophore did not compromise the mechanical performance of the actuator.

Each sample underwent two thermal cycles to guarantee reproducibility and repeatability. The thermomechanical tests were conducted on single-layer uniaxial actuators, with the director oriented along their long axis. The actuators had a thickness of approximately 100 μm and were subjected to a heating process from RT to 100 °C, followed by cooling down to RT. A 1 g load was applied to facilitate a more precise quantification of dimension changes, checking beforehand that this weight did not hinder the thermomechanical response of the actuators. Images were taken every 5 °C to measure the length (L) and width (W) of the actuator at each temperature, normalizing these values by the initial length (L_0) and

width (W_0) (see Fig. S3 for further details, ESI†). As shown in Fig. 2(c), the actuator started contracting noticeably at 35 °C, showing a 7% deformation at this temperature and reaching its maximum contraction of 40% at 75 °C. No further contraction was observed beyond this temperature. Upon cooling back to RT, the actuator fully recovered its original length. Contraction along the long axis was accompanied by a 20% expansion in the orthogonal direction at 75 °C, a phenomenon attributed to increased mesogenic disorder, as previously demonstrated.[13,32,36] To investigate whether the presence of the chromophore compromises the mechanical performance of the actuator, the same thermomechanical test was carried out on a control single-layer uniaxial LCE actuator prepared from a precursor ink analogous to the one used in this study, but without PO. The resulting deformation behavior, evaluated in terms of normalized length and width changes during thermal actuation, was comparable to that of the photothermal actuator. These results suggests that the incorporation of PO does not affect the mechanical behavior of the material (see Fig. S4, ESI†).

Radical formation process and reversibility (photochemistry assessment). As previously mentioned, the reprogrammability of these perylene diimide-containing LCE materials relies on the generation of radical species induced by green light.[18] For our purposes, it was essential to demonstrate that this process also takes place in this new polymeric matrix, which differs from the previous one in the type of reactive mesogens used in its formation. An analysis of the UV-Vis spectroscopic properties of a single-layer uniaxial actuator (100 μm thick) before and after green light irradiation revealed the appearance of new absorption bands in the far-red and near-infrared regions, along with a reduction in the original absorption peak around 530 nm (Fig. 2(d)), as previously reported for homologous materials.[18] Subsequent irradiation with 740 nm light caused these new bands to disappear, restoring the main absorption peaks associated with the perylene diimide chromophore to their original intensity, with deviations of less than 1%. Similarly, keeping the sample in the dark for 60 minutes also resulted in full spectral recovery, with the absorption profile reverting to its original state.

Considering that far-red light irradiation induces significant photothermal effect in these perylene systems (*vide infra*), the effect of the temperature on the radicals was assessed. For this purpose, we compared the evolution of the absorption spectrum of two actuators sensitized to far-red light over time, one kept at RT, while the other one was heated to 80 °C. As can be seen in Fig. S5 (ESI†), after 5 min, the actuator at RT exhibited a 14% loss of the height at its absorption peak (530 nm), while the one heated to 80 °C had recovered almost all of it, with a loss of only 3%. These results indicate that elevated temperatures significantly accelerate the thermal recovery of the absorption features in the material.

To confirm the formation of radical species, electron paramagnetic resonance (EPR) measurements were performed. The EPR spectrum revealed a single absorption feature after green light irradiation (centered at *ca.* g = 2.00 and about 0.5 mT broad). This signal was completely erased upon subsequent far-red light irradiation, as shown in Fig. 2(e). These EPR results clearly demonstrate the intrinsic association between radical species formation and green light irradiation.

To assess the cyclic stability of this radical formation process, the material was subjected to multiple cycles of green light irradiation followed by far-red light exposure. The UV-Vis results, shown in Fig. S6 (ESI†), demonstrate that the main absorption peak at around 530 nm decreased by approximately 15% after 20 cycles. However, the material retained a strong absorption in the green region (close to an absorbance of 2), providing sufficient radical generation capacity for subsequent photoinduced heating with far-red light irradiation.

Given the thermally reversible nature of the radical species, we investigated the effect of temperature on an actuator previously subjected to the same 20 cycle protocol. Following a 10-minute thermal treatment at 80 °C, the decrease in the 530 nm peak was reduced to just 7%, as shown in Fig. S7 (ESI†). To evaluate whether full spectral recovery could occur, the sample was evaluated again after 24 hours at ambient conditions, revealing complete restoration of the original spectrum.

Together, these results confirm that radical formation in our LCE matrix is initiated by green light and is reversible through far-red light and/or thermal treatment, with full spectral recovery observed under ambient conditions.

Material performance in terms of sensing, planning and actuation

As mentioned, the primary objective of this work is the integration of sensing, planning, and actuation within a reprogrammable single-material soft actuator, advancing toward a sorting soft robot. Therefore, it is crucial to characterize the performance of the material in response to light at the two employed wavelengths, as this will enable us to draw an analogy between the response of the system to these light stimuli and the three stages of the sense-plan-act paradigm mentioned above.

The ability of the LCE to transform green light absorption into radical species formation can be considered as the sensitivity of the material in this context. This sensitivity enables the system to gather information on the light transmission properties of the object to be sorted, thereby effectively sensing its characteristics. The presence or absence of radical species, triggered by green light, represents the registration of this information and dictates the specific plan for subsequent actuation based on the received light pattern. Notably, the material retains this information, storing the planned motion for later execution when stimulated with far-red light. In this way, the formation of long-lasting radical species functions as a memory of the plan to execute. Finally, far-red light activates the stored planned motion, facilitating object sorting based on their green light transmission properties. To ensure device effectiveness, a solid understanding of its mechanical performance under far-red light is essential. This includes assessing the ability of the system to perform the necessary non-reciprocal motions and exert sufficient mechanical force on the object to effectively accomplish the sorting task.

First, to gain deeper insight into the sensing step, a uniaxial actuator with a thickness of 70 μm was exposed to green light

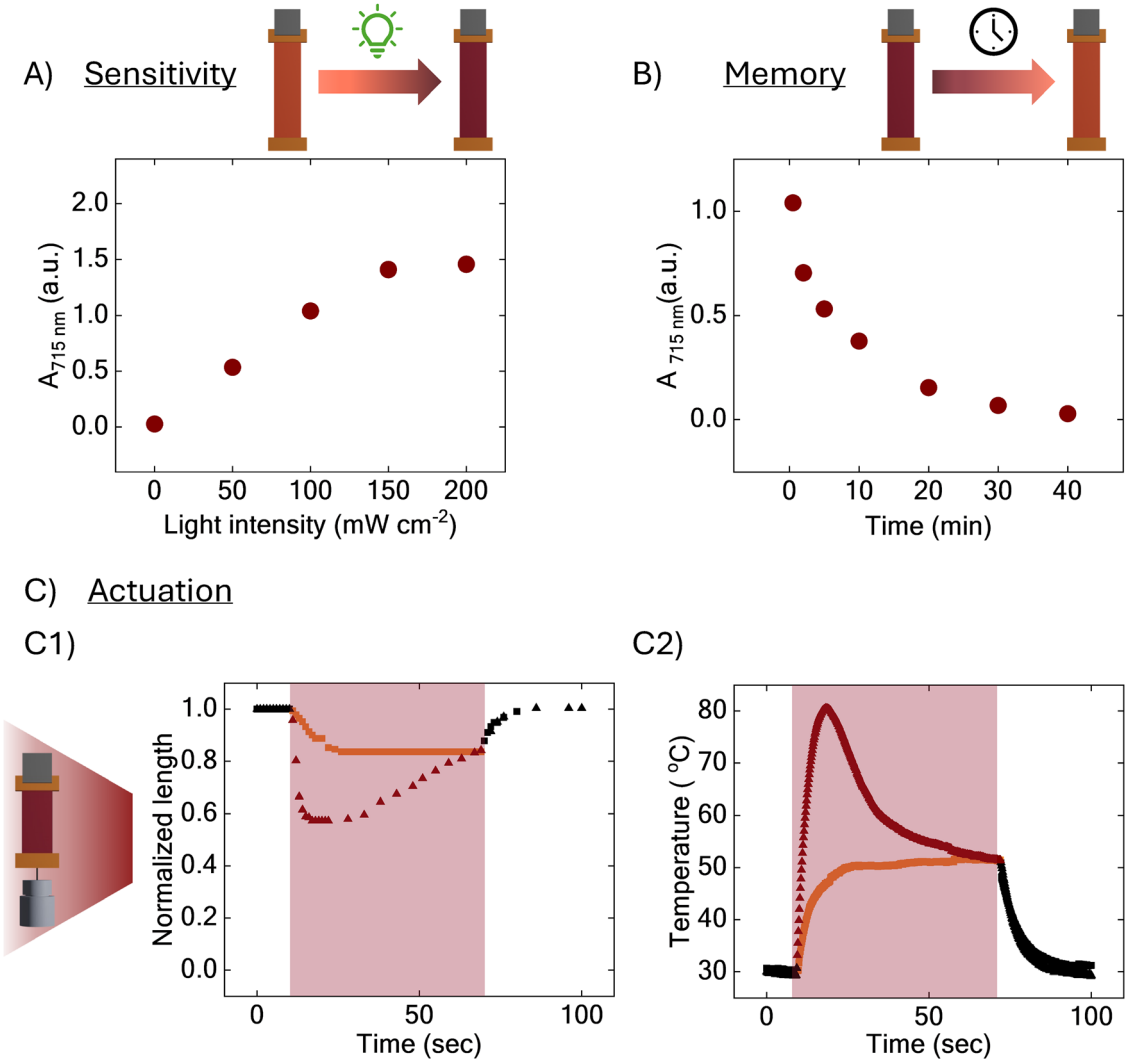

Fig. 3 Material performance: sensing, planning and actuation. (a) Absorption at 715 nm recorded for a single layer actuator (70 μm thick) after 30 seconds of irradiation with green light at intensities ranging from 50 to 200 mW cm^{-2}. The absorption of the actuator without prior green light exposure (0 mW cm^{-2}) is shown as a reference. (b) Decay of absorption at 715 nm over time for the same LCE actuator following 30 seconds of green light irradiations at 100 mW cm^{-2}. (c) Photoresponse of a single-layer uniaxial LCE actuator under far-red light illumination, with the director uniaxially aligned along its long axis and a 1g weight attached to its free end. The response is compared in both its unsensitized state and its sensitized state (after 30 seconds of green light irradiation at 100 mW cm^{-2}). (i) Temporal variation of the normalized strip length under far-red illumination at 400 mW cm^{-2} for both the unsensitized (orange squares) and sensitized (deep red triangles) states. When far-red illumination is turned off, the sample returns to its original length in both cases: unsensitized (black squares) and sensitized (black triangles). (ii) Time evolution of sample temperature under far-red illumination at 400 mW cm^{-2} for the unsensitized (orange squares) and sensitized (deep red triangles) states. When far-red illumination stops, the sample temperature returns to RT in both cases: unsensitized (black squares) and sensitized (black triangles).

for 30 seconds at intensities ranging from 50 to 200 mW cm^{-2}. This irradiation led to the formation of new absorption bands in the far-red region, with the highest peak observed at 715 nm. The absorption at this wavelength was recorded and is plotted in Fig. 3(a). This graph reveals that as the intensity of green light increased while maintaining a constant irradiation time, the absorption in the far-red region also increased. However, beyond 150 mW cm^{-2}, the growth of the absorption band at 715 nm exhibited a saturation effect, with no significant further increase. This suggests that at intensities above 150 mW cm^{-2}, radical species formation reached a plateau. A light intensity of 100 mW cm^{-2} was found to generate enough radical formation while keeping photoinduced heating low, as evidenced by the small contraction observed during the sensitization step (see Fig. S8, ESI†). For this reason, this intensity was chosen for the rest of the study.

As mentioned, the presence of long-lasting radicals can be understood as a form of memory within the material. These radicals effectively store information by maintaining a specific pattern that reflects the exposure of the material to green light. A crucial factor in this process is the stability of these radicals, as it determines how long the material can retain information before the radicals fade. To quantify this memory durability, we used the green light irradiation conditions established in

the previous experiment (30 seconds at 100 mW cm^{-2} light) and monitored the time evolution of the absorption at the 715 nm band, as shown in Fig. 3(b), following irradiation. This absorption is associated with the photothermal effect triggered upon switching on the far-red light. After 10 minutes following green light irradiation, the absorption at 715 nm decreased to 40% of its initial value, as measured immediately after exposure. For times exceeding tens of minutes after the green illumination step, far-red absorption was no longer sufficient to induce a significant photothermal effect. The memory durability was also studied under EPR tests, as shown in Fig. S9 (ESI†). The time evolution observed correlates with that obtained with the UV-Vis-NIR signal at 715 nm registered. The obtained results corroborate the long-lasting memory of the sensitization effect of the green light signal.

As a final key aspect of our actuator, we assessed the ability of the material to actuate under far-red light following prior green light irradiation. Fig. 3(c) shows the normalized length and temperature evolution over time for the single-layer uniaxial actuator when exposed to far-red light (400 mW cm^{-2}). The experiment was conducted first in its unsensitized state, without prior green light exposure, and then in its sensitized state, following green light irradiation.

In the unsensitized state, the actuator reached a maximum contraction of 17% within a few seconds upon far-red light exposure. This contraction is associated with the temperature increase of the LCE element from RT to 50 °C, which remained stable throughout the far-red light irradiation step. Once the far-red light was turned off, the system returned to its initial length within 6 seconds and rapidly cooled down back to RT. In contrast, when the actuator was sensitized by prior green light exposure, far-red light irradiation induced a rapid contraction of 43% within 6 seconds. This deformation then gradually decreased to around 20% over 40 seconds, approaching the contraction values observed in the unsensitized actuator. Once the far-red light source was turned off, the actuator fully recovered its original length within a few seconds, just as in the unsensitized state.

Overall, the prepared LCE material demonstrates sufficient sensitivity to moderate green light intensities (100 mW cm^{-2}), enabling the generation of a significant concentration of perylene radicals that strongly absorb in the far-red region, leading to substantial heating of the sensitized sample. These radicals persist for several minutes, providing memory to the system and sufficient time for operation. Additionally, the material exhibits a strong mechanical response at moderate temperatures (between RT to 70 °C) and undergoes rapid photoinduced heating under far-red light irradiation (400 mW cm^{-2}). In its unsensitized state, it contracts by 17%, while in the sensitized state, it contracts even faster and to a significantly greater extent (43%). These material properties, combined with optimized illumination conditions, establish a solid foundation for implementing the sorting robot.

Single-material sorting robot

With the described perylene-based material platform, we have undertaken the implementation of a photo-driven soft robotic sorting system using a single-material actuator. As outlined in the soft robot design section, we selected a 4D printed bimorph LCE actuator with layers having two orthogonal alignment directions within the plane, as a system to move the objects being sorted. As previously mentioned, these perylene diimide-based bimorph actuators sensitized with green light enable non-reciprocal motions, unlike unsensitized systems, which exhibit reciprocal motion.[18] Fig. 4(a) presents a series of stacked images capturing the bending of the actuator under far-red light irradiation (400 mW cm^{-2} for 12 seconds). These images compare its behavior in both the unsensitized (Fig. 4(a)-(i)) and the far-red sensitized states (Fig. 4(a)-(ii)), where only the free-tip half of the actuator was pre-irradiated with green light before far-red photoactuation, to induce the desired non-reciprocal motion. Fig. 4(a) also presents the unbending process when far-red light is switched off for both states. Additionally, Fig. 4(b) plots the trajectory of the actuator tip during bending and unbending. For further details on these movements, see Movies S1 and S2 (ESI†).

From the photoinduced bending experiment in Fig. 4(a)-(i), we conclude that the unsensitized actuator bends steadily to the right (toward higher positive x-values) until the end of the far-red irradiation step. During this motion, the tip first reaches its maximum height before continuing to shift rightward. In contrast, the sensitized actuator exhibits a notably different bending behavior. The free-tip half, which was previously irradiated with green light, bends more rapidly, with more pronounced curvature under far-red irradiation than the other half, the one closer to the anchor, that was not pre-exposed to green light. This untreated half bends more slowly, following the typical dynamics of an unsensitized actuator. Consequently, as seen in Fig. 4(a)-(ii), the maximum height h_s reached during bending by the sensitized actuator is significantly less (3.4 mm lower) than that of the unsensitized actuator.

The far-red light intensity and exposure duration were selected based on two key considerations. First, the irradiation should be sufficiently long to induce significant bending in the unsensitized actuator, leading to a notable increase in its height and a steady rightward shift of its tip. Second, the duration should allow the sensitized actuator to complete its strong bending phase, following a trajectory that remains distinctly lower than the unsensitized actuator. Specifically, irradiation was stopped once the sensitized actuator made a closed loop, ensuring a clear distinction in movement dynamics (see Fig. 4(a)-(ii) and Movie S2, ESI†). Based on these considerations, we have set the far-red light intensity at 400 mW cm^{-2} for 12 seconds, as it effectively balances both requirements.

When the far-red light is switched off, the heating stimulus ceases, causing the sample to rapidly cool down and unbend to its relaxed state at RT. In both, the unsensitized and sensitized states, the actuator returns to its original position, but their unbending trajectories differ. The tip of the unsensitized actuator follows nearly the same path in reverse as during bending (see Fig. 4(b)). In contrast, the sensitized actuator follows a distinct unbending trajectory compared to its bending

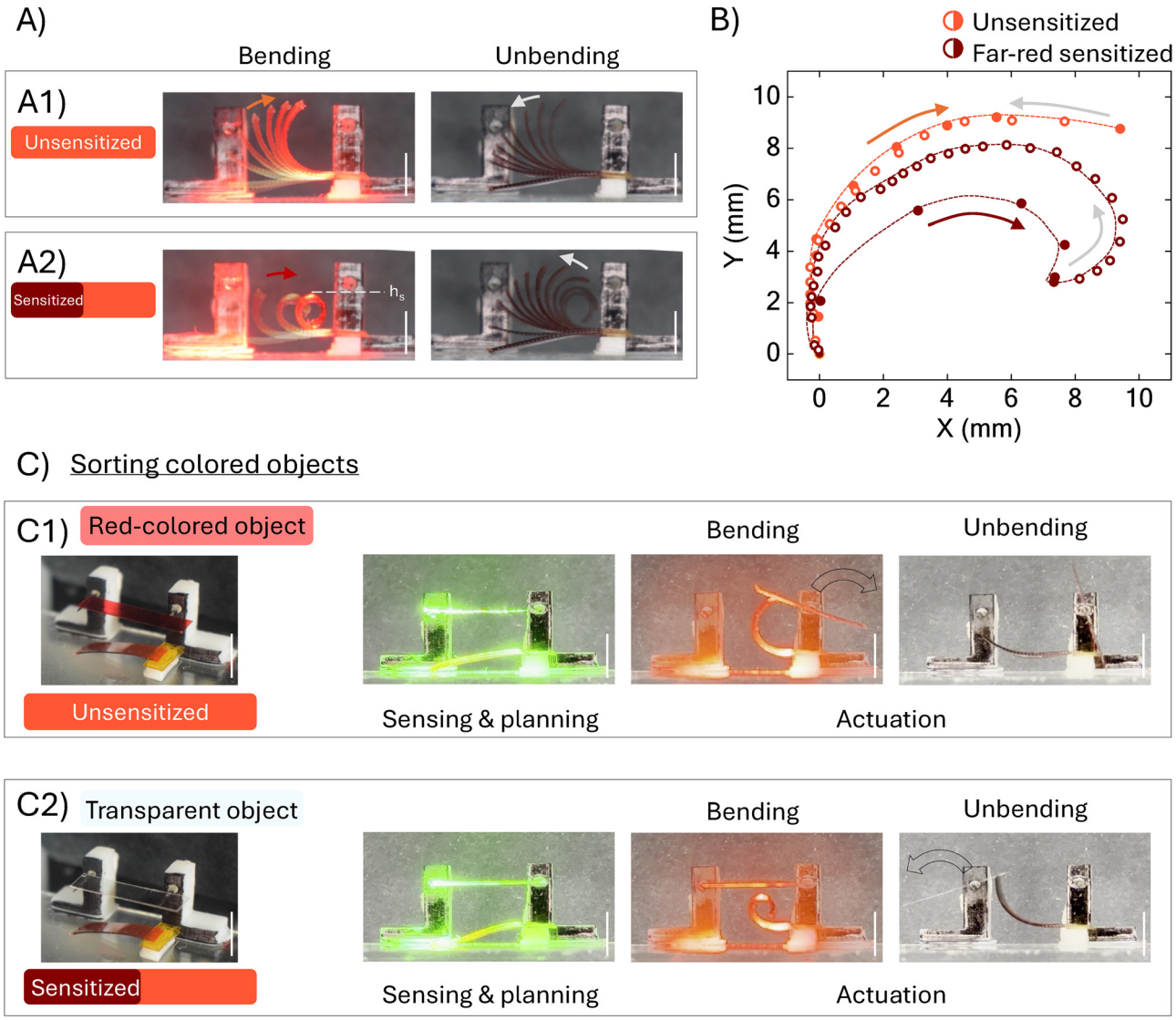

Fig. 4 Sorting soft robot based on a reprogrammable photosensitive LCE. (a) Stacked images showing the bending and unbending behavior of a 4D printed bimorph LCE actuator under far-red light (400 mW cm^{-2} for 12 seconds). (i) Unsensitized actuator. (ii) Far-red sensitized actuator, where only the free-tip half was pre-irradiated with green light (100 mW cm^{-2} for 30 seconds), to induce the desired non-reciprocal motion. Under far-red irradiation, the actuators bend and return to their relaxed state once the light is turned off. Scale bar represents 5 mm. (b) Comparison of the tip trajectories of a 4D printed bimorph LCE actuator under far-red light irradiation. The *XY* coordinates of the actuator tip are plotted for both the unsensitized (orange) and far-red sensitized (deep red) states. Solid circles represent the bending trajectory, while hollow circles indicate the unbending phase. In the unsensitized actuator, the bending and unbending trajectories overlap due to the characteristic reciprocity of the movement. Note that lines are drawn to guide the eye. (c) Autonomous sorting of sheets based on their green-light transmission properties. The irradiation sequence and experimental geometry are the same for both experiments (same irradiation condition as above): (i) when a red sheet is placed, green light is blocked, preventing the 4D printed bimorph LCE actuator from becoming sensitized to far-red light. As a result, during far-red irradiation, the actuator bends uniformly, touching and pushing the sheet to the right. When the far-red light is switched off, the actuator unbends returning to the original position. (ii) When a transparent object is placed, green light passes through, sensitizing the LCE actuator to far-red light. During far-red irradiation, the half of the actuator closer to the anchor bends similarly to the unsensitized actuator, however, the free half exhibits a more pronounced curvature, passing below the transparent object. When far-red light is switched off, the actuator unbends, pushing the transparent sheet to the left, effectively sorting it to the opposite side. Scale bar represents 5 mm.

phase. Upon far-red light removal, the tip of the sensitized actuator first shifts toward higher positive *x*-values (*i.e.*, to the right) until reaching a maximum point. After this, the tip steadily moves toward decreasing *x*-values (*i.e.*, to the left), with its trajectory advantageously converging with that of the unsensitized actuator and reaching heights significantly greater than those achieved during bending. Eventually, both actuators return to their original state (see Fig. 4(b)).

By closely examining the trajectories of the actuator for both states, under identical far-red light stimulation, followed by a period with no irradiation, a key difference emerges. During bending, the sensitized actuator maintains a notably lower

trajectory, remaining always below a critical height, defined in Fig. 1(d)-(ii) as h_s, until irradiation ends, whereas the unsensitized actuator surpasses this critical height, steadily increasing in height while moving to the right. The sensitized actuator, in contrast, surpasses this height only during unbending while moving to the left. This dual-mode actuation feature allows for differentiated object interaction as shown below.

If an object is placed just above the critical height h_s of the sensitized actuator during the bending stage, the actuator interacts with it differently. The unsensitized actuator contacts the object during bending and, if its force is sufficient, pushes it to the right. Meanwhile, the sensitized actuator bends below the object without touching it but eventually contacts it during unbending, moving it to the left if the force is sufficient. Since the only difference between the actuators is the exposure of its free-tip half to green light, this system provides a mechanism to autonomously sort objects based on their light-transmitting properties. Objects such as sheets, placed above the defined critical height h_s, can potentially be sorted depending on their ability to either block or allow green light transmission.

Fig. 4(c)-(i) shows the system in which a red sheet is positioned slightly above the critical height h_s, placed between the actuator and the green light source. When the green light is switched on, it is absorbed by the red sheet, preventing it from reaching the actuator and keeping it in the unsensitized state (see Fig. S10, ESI†). Upon far-red light irradiation from below, the actuator contacts the sheet during the bending process and effectively moves it to the right. By an appropriate design of the sheet holder, this movement is sufficient to make the sheet fall toward the right as shown in Movie S3 (ESI†). When the far-red light is switched off, the actuator returns to its relaxed RT state.

Under the same illumination sequence, if a transparent sheet is placed on the holder at the same position, green light passes through it, sensitizing the free-tip half of the actuator to far-red light (see Fig. 4(c)-(ii)). Upon far-red illumination, this region bends more strongly due to the enhanced absorption by radical species in the patterned actuator. As a result, it remains below the critical height h_s during the bending phase, passing below the transparent sheet. When the far-red light stimulus is removed, the actuator quickly unbends and surpasses the critical height h_s, while steadily moving to the left, eventually contacting the sample and effectively moving it leftward, as shown in Movie S4 (ESI†). It is worth noting that the presence of the sheet ($\sim$5 mg) has a negligible effect on the trajectory of the actuator, as seen in Movies S1–S4 (ESI†). However, significantly larger masses may impact performance and limit scalability. In any case, this work is intended solely as a proof of concept of the sorting potential of our system.

Importantly, the actuator is reusable, being capable of continuous operation. For objects that block green light, like our red sheet, no radicals are formed, being the actuator immediately available for subsequent sorting cycles without further treatment. However, after sorting a green-light-transmissive object, like the transparent sheet, a sufficient dose of far-red illumination is needed to deplete the radical species generated, restoring the actuator to its initial, radical-free state, ready for reuse in the next sorting event. This reset step is needed to ensure consistent deformation trajectories between cycles, minimizing variability due to incomplete radical depletion. This feature, validated through several cycles of non-reciprocal motion (see Fig. S11, ESI†), demonstrates repeatable performance of the actuator under the selected irradiation scheme, making the system suitable for continuous autonomous sorting tasks. To enable such continuous operation, the system would require precise synchronization of green and far-red light irradiation steps, automated object delivery to the actuator, and a sufficient far-red illumination time that fully erase residual radicals after sorting green-light-transmissive objects. By incorporating these elements, namely, controlled optical programming, automated object handling and radical reset, the LCE actuator could be embedded into a fully autonomous sorting platform capable of sustained operation.

Conclusions

In this work, we have demonstrated a single-material LCE-based photo-actuator capable of autonomously sorting objects based on their green-light transmission properties. To implement it we have leveraged the advantages of 4D-printable, perylene-doped liquid crystal elastomers, which offer a dual functionality: they enable precise mechanical control through director engineering *via* 4D printing, and tunable photo-response through patterned green illumination. Specifically, exposure to green light generates radical species that strongly absorb in the far-red region. By precisely controlling the spatial distribution of these radicals through patterned illumination, we achieve accurate and reprogrammable multi-mode mechanical actuation.

By carefully designing the system and the illumination conditions, we enable the actuator to sense the green light transmission properties of the object to sort through the localized formation of radical species on it. The specific spatial radical patterns produce distinct actuator responses for green-light-transmissive and non-transmissive objects, even under identical far-red light illumination conditions. This dual-mode response allows differentiated object interaction. Specifically, objects that block green light prevent radical formation in the actuator, resulting in a mechanical deformation under far-red illumination that moves the object in one predefined direction. Conversely, green-light-transmissive objects allow radical formation in a specific part of the actuator, triggering a distinctly different deformation that moves the object in the opposite direction. This dual-mode actuation mechanism enables objects to be autonomously sorted solely according to their green-light transmission properties. Importantly, the actuator is optically resettable, being capable of continuous operation.

Overall, our single-material reprogrammable actuator integrates sensory input to modulate its response, providing it with a deliberative decision-making capability rather than a reactive behavior, characteristic of conventional LCE-based self-regulated systems.

Our reprogrammable actuator senses the green-light transmission properties of the object to be sorted through localized radical generation and encodes an actuation plan dictating its subsequent deformation under far-red light irradiation. This step works as a physically embedded, algorithm-like process, where the material itself processes an optical input and translates it into a programmed mechanical response. As a result, objects with different optical properties trigger distinct actuation modes, enabling autonomous sorting. In addition, the actuator exhibits reversible and reproducible behavior over multiple cycles, with stable photomechanical performance, supporting its potential for continuous use. By combining perylene-based LCE reprogrammability and engineered director morphology, our system integrates sensing and elementary deliberative decision-making capabilities, providing a level of autonomy to LCE-based soft robotics that marks a step forward toward the widely pursued sense–plan–act paradigm.

Author contributions

Lorena Montesino: conceptualization, methodology, investigation, writing (original draft), writing (review and editing); María López-Valdeolivas: investigation, writing (review and editing); Jesús I. Martínez: investigation, writing (review and editing); Carlos Sánchez-Somolinos: conceptualization, methodology, investigation, writing (original draft), writing (review and editing), funding acquisition.

Data availability

The data that support the findings of this study are available from the corresponding author upon reasonable request.

Conflicts of interest

There are no conflicts to declare.

Acknowledgements

The described research is part of the project PRIME. This project has received funding from the European Union's Horizon 2020 research and innovation programme under Grant Agreement No 829010 (PRIME). Funding has also been received from Spanish "Ministerio de Ciencia, Innovación y Universidades (MCIU)" through AEI/FEDER(UE) PID2020-118485RB-I00 and PID2022-140923NB-C21, Gobierno de Aragón project PROY_E28_24, FEDER (EU) and Fondo Social Europeo (DGA E15_20R and E09_23R). This research was also supported by CIBER-Consorcio Centro de Investigación Biomédica en Red-(CB06/01/00263), Instituto de Salud Carlos III, Ministerio de Ciencia e Innovación. L. M. acknowledges Gobierno de Aragón for a predoctoral fellowship (2020–2024). C. S. S. acknowledges FAB3D interdisciplinary platform (PTI-CSIC) for support.

References

1 A. F. T. Winfield, *Robotics: a very short introduction*, Oxford Univ. Press, Oxford, 1st edn, 2012.
2 B. Siciliano, L. Sciavicco, L. Villani and G. Oriolo, *Robotics*, Springer, London, 2009.
3 P. Corke, *Robotics, Vision and Control*, Springer Berlin Heidelberg, Berlin, Heidelberg, 2011, vol. 73.
4 C. Majidi, *Adv. Mater. Technol.*, 2019, **4**, 1800477.
5 H. Zeng, P. Wasylczyk, D. S. Wiersma and A. Priimagi, *Adv. Mater.*, 2018, **30**, 1703554.
6 P. Lyu, M. O. Astam, C. Sánchez-Somolinos and D. Liu, *Adv. Intell. Syst.*, 2022, **4**, 2200280.
7 O. M. Wani, R. Verpaalen, H. Zeng, A. Priimagi and A. P. H. J. Schenning, *Adv. Mater.*, 2019, **31**, 1805985.
8 B. Mazzolai, A. Mondini, E. Del Dottore, L. Margheri, F. Carpi, K. Suzumori, M. Cianchetti, T. Speck, S. K. Smoukov, I. Burgert, T. Keplinger, G. D. F. Siqueira, F. Vanneste, O. Goury, C. Duriez, T. Nanayakkara, B. Vanderborght, J. Brancart, S. Terryn, S. I. Rich, R. Liu, K. Fukuda, T. Someya, M. Calisti, C. Laschi, W. Sun, G. Wang, L. Wen, R. Baines, S. K. Patiballa, R. Kramer-Bottiglio, D. Rus, P. Fischer, F. C. Simmel and A. Lendlein, *Multifunct. Mater.*, 2022, **5**, 032001.
9 M. O. Astam, S. A. M. Weima, T.-H. Lee, A. Van Bezouw and D. Liu, *Matter*, 2024, **7**, 1785–1798.
10 M. Winkler, A. Kaiser, S. Krause, H. Finkelmann and A. M. Schmidt, *Macromol. Symp.*, 2010, **291–292**, 186–192.
11 E. R. Espíndola-Pérez, J. Campo and C. Sánchez-Somolinos, *ACS Appl. Mater. Interfaces*, 2024, **16**, 2704–2715.
12 S. Schuhladen, F. Preller, R. Rix, S. Petsch, R. Zentel and H. Zappe, *Adv. Mater.*, 2014, **26**, 7247–7251.
13 M. López-Valdeolivas, D. Liu, D. J. Broer and C. Sánchez-Somolinos, *Macromol. Rapid Commun.*, 2018, **39**, 1700710.
14 M. Wang, S. M. Sayed, L.-X. Guo, B.-P. Lin, X.-Q. Zhang, Y. Sun and H. Yang, *Macromolecules*, 2016, **49**, 663–671.
15 W. Zhang, Y. Nan, Z. Wu, Y. Shen and D. Luo, *Molecules*, 2022, **27**, 4330.
16 L. Ceamanos, Z. Kahveci, M. López-Valdeolivas, D. Liu, D. J. Broer and C. Sánchez-Somolinos, *ACS Appl. Mater. Interfaces*, 2020, **12**, 44195–44204.
17 L. Ceamanos, D. J. Mulder, Z. Kahveci, M. López-Valdeolivas, A. P. H. J. Schenning and C. Sánchez-Somolinos, *J. Mater. Chem. B*, 2023, **11**, 4083–4094.
18 L. Montesino, J. I. Martínez and C. Sánchez-Somolinos, *Adv. Funct. Mater.*, 2024, **34**, 2309019.
19 P. Sartori, R. S. Yadav, J. Del Barrio, A. DeSimone and C. Sánchez-Somolinos, *Adv. Sci.*, 2024, 2308561.
20 W. Liao and Z. Yang, *Adv. Mater. Technol.*, 2022, **7**, 2101260.
21 J. Jiang and Y. Zhao, *Small*, 2023, **19**, 2301932.
22 J. Min, Z. Wu, W. Zhang, Y. Liu and D. Luo, *Adv. Sens. Res.*, 2024, **3**, 2300117.
23 S. Zhou, Y. Li, Q. Wang and Z. Lyu, *Cyborg Bionic Syst.*, 2024, **5**, 0105.
24 O. M. Wani, H. Zeng and A. Priimagi, *Nat. Commun.*, 2017, **8**, 15546.
25 P. Lyu, D. J. Broer and D. Liu, *Nat. Commun.*, 2024, **15**, 4191.

26 S. Li, M. M. Lerch, J. T. Waters, B. Deng, R. S. Martens, Y. Yao, D. Y. Kim, K. Bertoldi, A. Grinthal, A. C. Balazs and J. Aizenberg, *Nature*, 2022, **605**, 76–83.
27 M. Lahikainen, H. Zeng and A. Priimagi, *Nat. Commun.*, 2018, **9**, 4148.
28 M. Lahikainen, H. Zeng and A. Priimagi, *Soft Matter*, 2020, **16**, 5951–5958.
29 S. Tian, S. J. D. Lugger, C.-S. Lee, M. G. Debije and A. P. H. J. Schenning, *J. Am. Chem. Soc.*, 2023, **145**, 19347–19353.
30 A. H. Gelebart, D. J. Mulder, G. Vantomme, A. P. H. J. Schenning and D. J. Broer, *Angew. Chem., Int. Ed.*, 2017, **56**, 13436–13439.
31 W. Feng, Q. He and L. Zhang, *Adv. Mater.*, 2024, 2312313.
32 C. P. Ambulo, J. J. Burroughs, J. M. Boothby, H. Kim, M. R. Shankar and T. H. Ware, *ACS Appl. Mater. Interfaces*, 2017, **9**, 37332–37339.
33 T. S. Hebner, C. N. Bowman and T. J. White, *Polym. Chem.*, 2021, **12**, 1581–1587.
34 J. M. McCracken, B. R. Donovan, K. M. Lynch and T. J. White, *Adv. Funct. Mater.*, 2021, **31**, 2100564.
35 G. E. Bauman, J. M. McCracken and T. J. White, *Angew. Chem., Int. Ed.*, 2022, **61**, e20220257.
36 D. J. Broer and G. N. Mol, *Polym. Eng. Sci.*, 1991, **31**, 625–631.